# Calculations for electron impact ionization of Be atoms and its charged states, Be+ and Be2+


| | |
|---|---|
| journal or publication title | Journal of Physics B: Atomic, Molecular and Optical Physics |
| volume | 51 |
| number | 13 |
| page range | 135201 |
| year | 2018-07-14 |
| URL | http://hdl.handle.net/10655/00012961 |

doi: 10.1088/1361-6455/aac1ef

Creative Commons : 表示
http://creativecommons.org/licenses/by/3.0/deed.ja


# Calculations for electron impact ionization of Be atoms and its charged states, $Be^{+}$ and $Be^{2+}$

**G. Purohit[1,2] and D. Kato[1,3,4]**

[1]National Institute for Fusion Science, National Institutes of Natural Sciences 322-6 Oroshi-cho, Toki Gifu, 509-5292, Japan
[2]Department of Physics, Sir Padampat Singhania University, Bhatewar, Udaipur-313601, India
[3]Department of Fusion Science, SOKENDAI, 322-6 Oroshi-cho, Toki Gifu, 509-5292, Japan
[4]Department of Advanced Energy Engineering Science, Kyushu University, Kasuga Fukuoka, 816-8580, Japan

**Abstract**

Electron impact triple differential cross section (TDCS) results are reported for the single ionization of Be(2s), Be(1s), $Be^{2+}$(1s) and $Be^{+}$(2s) targets. The differential cross sections have been calculated in the modified distorted wave formalism under different kinematical conditions for the coplanar emission of electrons. Due to unavailability of experimental data, we have made a careful comparison of Be and it's ions TDCS with the trends of TDCS measured for He and Li targets, which have similar electronic configurations as $Be^{+2}$ and $Be^{+}$ respectively. Similarity in the trends of TDCS are observed for He(1s); $Be^{2+}$(1s) targets, Li(2s); $Be^{+}$(2s) and Be(1s); $Be^{2+}$(1s) targets. Effects of iso-electronic and iso-nuclear configurations on collision dynamics are observed in the trends of TDCS.

## I. Introduction

The electron impact ionization of targets such as atoms and ions has attracted attention of researchers from the early days of quantum mechanics. The electron impact ionization cross sections are essential in the modeling of plasma in fusion research, ionization mass spectrometry and astrophysical applications. Differential cross sections play an important role in self-consistent kinetic modeling of discharges having non-Maxwellian electron velocity distributions [1]. Beryllium (Be) is one of the materials which is directly exposed to the plasma components in the International Thermonuclear Experimental Reactor (ITER) [2, 3]. For ITER and other plasma facilities, three problems remain important namely; design of plasma facing components, proper selection of plasma facing materials and plasma-wall interactions. For the plasma facing materials, Be is an important candidate for the first wall since it is a low Z material which reduces the effect of impurities in the plasma. Formation of gas-phase Be in various charge states and of hydrides of Be, takes place when the erosion of Be walls occurs in contact with the hot plasma containing hydrogen and its isotopes [4, 5]. Electron collision processes on the beryllium and its charged states play an important role in the fusion edge and diverter plasmas. Extensive calculations have been done for the elastic, excitation and ionization cross sections of Be and its charged states such as convergent close-coupling (CCC) [6], R-matrix with pseudo states (RMPS) [7, 8] and time-dependent close coupling (TDCC) [9]. More theoretical studies for the electron impact processes, mainly excitation, on neutral Be may be summarized as; R-matrix [10], distorted-wave [11], RMPS [12] and CCC [13] calculations. Furthermore, recently the B-spline R-matrix and the convergent close coupling methods have been utilized to study electron collisions with neutral beryllium in the energy range from threshold to 100 eV [14].

Electron – $Be^+$ cross section data are also of interest in fusion research [15]. Theoretical studies have been reported for $Be^+$ in close coupling [16], R-matrix [17], distorted wave [11] and RMPS, CCC [18] approaches. Excitation process from the He like $Be^{+2}$ has been studied in the distorted wave [19, 20] and CCC [8] formalism. RMPS calculations [8, 21] have also been done for the electron impact excitation processes on $Be^{3+}$ ions. Detailed study of electron impact ionization cross sections have been reported for the Be isoelectronic ions using various theoretical approaches such as two potential distorted wave approximation [22], simplified improved binary-encounter dipole model (siBED) [23, 24], QIBED (with the ionic correction) and RQIBED (with both the ionic and relativistic corrections) [25].

Electron impact cross sections for beryllium and beryllium hydrides have also been reported recently [26]. Due to the toxic nature of beryllium, there has been technical difficulty in measurements and the experimental data reported have been very few. Experimental excitation data have been reported for the $2s \rightarrow 2p$ transition in $Be^+$ [27]. The double to single photoionization ratio have been measured for beryllium and it has been compared with the electron impact ionization cross sections of $Be^+$ [28]. Beryllium also belongs to the family of alkaline earth metals and following helium it is the most important closed shell atom. Differential cross section results, experimental as well as theoretical, have been reported for the other higher Z member of the alkaline earth metals such as Mg [29-31] and Ca [32-34]. To the best of our knowledge there are no differential cross section data available for the electron impact single ionization of the alkaline earth metal beryllium. However, triple differential cross

sections for the double photoionization of beryllium atoms from outer [35] as well as inner shell [36] have been reported. TDCS for the direct double photoionization of alkaline earth atoms including Be has been reported [37] and the structure of TDCS has been analyzed in comparison to helium atoms. Electron impact single ionization TDCS have been reported for the Li like ion, $Be^+$ [38]. Double ionization process from beryllium target has also been studied and electron impact fully differential cross sections have been calculated (see [39] and references cited in).

We report in this paper electron impact triple differential cross sections for the single ionization of Be(2s), Be(1s), $Be^{2+}$(1s) and $Be^+$(2s) targets. Present investigation has been done in the distorted wave Born approximation (DWBA) formalism to obtain the information about the collision dynamics of alkaline earth metal target Be. We have employed different kinematical conditions to obtain TDCS for the beryllium atoms and also its ions. Effect of target polarization potential and post collision interaction (PCI) have been included in the DWBA formalism for all the lower energy kinematical conditions, however the polarization potential and PCI is not expected to be very significant for the higher energy cases. We have also calculated inner shell ionization cross sections which help to understand the collision dynamics better. In absence of the measurements, even for the total cross sections, the theoretical cross section data are very much important for the application purposes. Present attempt is helpful to analyze the trends of TDCS as we have made a careful comparison of Be and it's ions TDCS with the trends of TDCS measured for He [40-41] and Li [42] targets. The theoretical TDCS results reported previously for the Li [43, 44] have also been compared with the trends of TDCS for $Be^+$. Next section summarizes the theoretical formalism used for the present calculations.

## II. Theory

In the electron impact single ionization process, an incident electron of linear momentum $k_0$ and energy $E_0$ ionizes the target (atom / ion) and the two emerging electrons are described by the linear momentum and energy ($k_1$, $E_1$) and ($k_2$, $E_2$), where the scattered (primary) electron is specified by subscript 1 and the ejected (secondary) electron is specified by subscript 2. The energy conservation principle states;

$$E_0 = E_1 + E_2 + E_b \quad (1)$$

where $E_b$ is the energy of the bound electron.

The TDCS for the electron impact single ionization, which is the probability of single ionization, is expressed in atomic units as

$$\frac{d^3\sigma}{d\Omega_1\, d\Omega_2\, dE_1} = (2\pi)^4 \frac{k_1 k_2}{k_0} \sum_{av} |T(k_1, k_2, k_0)|^2 \quad (2)$$

with

$$T(k_1, k_2, k_0) = \langle k_1 k_2 | T | \psi_{n1} k_0 \rangle .$$

The expression in Eq. (2) includes a sum over final and average over initial magnetic and spin state degeneracy. The T matrix in Eq.(2), which is the subject of approximation, includes interaction between the incident and target electrons and the nucleus.

The TDCS for the ionization from nl orbital is expressed in terms of direct and exchange scattering amplitudes as;

$$\frac{d^3\sigma}{d\Omega_1\, d\Omega_2\, dE_1} = (2\pi)^4 \frac{k_1 k_2}{k_0} \sum_{m=-l}^{l} \left( |f_{nlm}|^2 + |g_{nlm}|^2 - \mathrm{Re}\left( f_{nlm}^{*}\, g_{nlm} \right) \right) \tag{3}$$

where

$$f_{nlm} = \left\langle X_1^{(-)}(k_1, r_1)\, X_2^{(-)}(k_2, r_2) \left| v_3 \right| X_0^{(+)}(k_0, r_1)\, \psi_{nl}(r_2) \right\rangle, \tag{4}$$

$$g_{nlm} = \left\langle X_1^{(-)}(k_1, r_2)\, X_2^{(-)}(k_2, r_1) \left| v_3 \right| X_0^{(+)}(k_0, r_1)\, \psi_{nl}(r_2) \right\rangle \tag{5}$$

here $v_3 = \dfrac{1}{|r_1 - r_2|}$ is the interaction potential between the incident and target electron responsible for the ionization, the radial coordinate $r_1$ initially represent the incident or projectile electron which is scattered after the collision. The distorted wave function for the incident electron is represented by $X_0^{(+)}(k_0, r_1)$. $X_1^{(-)}(k_1, r_1)$ and $X_2^{(-)}(k_2, r_2)$ represent the distorted wave functions for the two outgoing electrons and each is orthogonalized with respect to $\psi_{nl}$. Equations (4) and (5) are direct and exchange amplitudes for ionization from the $(n, l)$ shell of the target atom where $\psi_{nl}$ is the corresponding target orbital from which the ionization is taking place, and $n$ and $l$ are the principal and orbital quantum numbers respectively. We have used Hartree-Fock orbitals of Clementi and Roetti [45] for $\psi_{nl}$. For the work reported here we have made a careful check to ensure that the cross sections converge satisfactorily for the number of partial waves used. To calculate the distorted wavefunction we have used the spin-averaged static-exchange potential (SASEP) of Furness and McCarthy [46] as modified by Riley and Truhlar [47], which is given as

$$V_E(r) = 0.5[E_0 - V_D(r) - \{[E_0 - V_D(r)]^2 + 4\pi\rho(r)\}^{1/2}] \tag{6}$$

where $\rho(r)$ is the electron density.

The direct distorting potential $V_D(r)$ for the incident electron is obtained from the target radial orbital $u_{nl}(r)$ [48] as

$$V_D(r) = -\frac{Z}{r} + \sum_{nl} N_{nl} \int dr' [u_{nl}(r')]^2 / r_> \quad (7)$$

where $r_>$ is the greater of $r$ and $r'$. The equivalent local ground state potential U, which is the sum of exchange and direct potentials, and expressed as follows;

$$U = V_D(r) + V_E(r), \quad (8)$$

The initial-state distorted waves $X_0^{(+)}(k_0, r_1)$ are generated in the equivalent local ground state potential of the atom. The final-state distorted waves $X_1^{(-)}(k_1, r_1)$ and $X_2^{(-)}(k_2, r_2)$ are obtained in the equivalent local ground state potential of the ion. For the lower energy cases the TDCSs have been calculated by including correlation-polarization potential $V_{CP}(r)$ in the distorting potential (Eq. 8). The correlation-polarization potential $V_{CP}(r)$ is given as follows;

$$\begin{aligned} V_{CP}(r) &= V_{SR}^{Corr}(r), \quad r \le r_0 \\ &= -\frac{\alpha_d}{2r^4}, \qquad r > r_0 \end{aligned} \quad (9)$$

where the fundamental form of the short range correlation and long range polarization potential has been approximated by means of local density functional theory [49, 50]. $\alpha_d$ is dipole polarizability of the target and $V_{SR}^{Corr}(r)$ is short range correlation potential [49]. The point $r_0$ is the intersection of the short range correlation and long range polarization potential, we have ensured the smooth matching of potentials at $r_0$. The post collision interaction (PCI) has been calculated using the Ward-Macek factor ($M_{ee}$) [51], the $M_{ee}$ is defined as

$$M_{ee} = N_{ee} \left| {}_1F_1(-i\lambda_3, 1, -2k_3 r_{3ave}) \right|^2, \quad (10)$$

where

$$Nee = \frac{\gamma}{e^{\gamma} - 1}, \gamma = -\frac{2\pi}{|k_1 - k_2|}, \lambda_3 = -\frac{1}{|k_1 - k_2|}, k_3 = \frac{1}{2}|k_1 - k_2|, \; r_{3ave} = \frac{\pi^2}{16\varepsilon}\left(1 + \frac{0.627}{\pi}\sqrt{\varepsilon}\ln\varepsilon\right)^2$$

with

$\varepsilon = (k_1^2 + k_2^2)/2$ being the total energy of the exiting electrons.

The DWBA approach with inclusion of target polarization and PCI has been successful to describe the low energy ionization from various atomic and molecular targets and considering the ionization taking place from one electron orbital, bound target state constructed from Hartree-Fock orbitals [45], has also been reasonably good to describe the features of TDCS (see [52] and references cited in). The present theoretical approach may be expected to give reasonable estimates for the ionization of targets with 1s and 2s orbitals. The results and discussion is summarized in the next section.

## III. Results and Discussion

The triple differential cross sections results for the electron impact single ionization of Be(2s), Be(1s), $Be^{2+}$(1s) and $Be^{+}$(2s) targets are presented in Figures 1-7. The results of TDCS for Be(2s) atoms at incident electron energy 31.0 eV are presented in Figure 1. The TDCSs have been calculated at ejected electron energy 2.0 eV for different values of scattering angles, namely $2^0$ (Fig. 1a), $5^0$ (Fig. 1b) and $10^0$ (Fig. 1c). The TDCSs for helium atom have also been calculated for the similar kinematic conditions for comparison of the trends of TDCS (Fig. 1d). The solid curves represent TDCSs calculated in DWBA formalism including polarization potential and PCI and the dashed curves represent TDCSs calculated in standard DWBA. Apart from binary and recoil peaks two more peaks are observed in the TDCS trends for beryllium atoms. The binary and recoil peaks are observed in the direction of momentum transfer and its opposite (shown by arrows in Figure 1), however the peaks are shifted towards higher values of ejected electron angles for higher momentum transfer (i.e. higher scattering angles) in the standard DWBA results (dashed curves). The value of momentum transfer (K) is obtained by the relation $\mathrm{K} = |\mathbf{k_0} - \mathbf{k_1}|$, where $k_0$ and $k_1$ are the momenta of incident and scattered electrons respectively. The DWBA results including target polarization potential and post collision interaction (PCI) produce shift in the peak positions as well as changes in the magnitude of peaks (solid curves in Figs. 1b and 1c). The recoil to binary peak ratio increases with increase in the scattering angle and the magnitude of peak observed near ejected electron angle $\theta_2 = 300^0$ decreases. Presence of extra peaks in the TDCS structure of beryllium atoms may be attributed to the radial node of 2s wave function, the difference in the trends of TDCS for the ionization from 1s orbital is visible from the TDCS plotted for helium target (Fig. 1d). The PCI is too strong for the forward and backward ejected electron angles which makes the TDCS nearly zero around $\theta_2 = 0^0 \text{ and } 360^0$ and also shifts the peak positions for helium atoms (solid curve in Fig. 1d).

TDCS results for the inner shell ionization of beryllium atoms (i.e. ionization from Be(1s)) are presented in Figure 2. The DWBA results have been obtained for ejected electron energy 2 eV at incident electron energies 200 eV, 500 eV and 1000 eV for scattering angles $2^0$ (solid curve), $5^0$ (dashed curve) and $10^0$ (dotted curve). The polarization and PCI have not been found significant at the incident electron energies used so only standard DWBA results are displayed. Very strong recoil peak is observed at incident electron energy 200 eV (Fig. 2a). The smaller binary peak is observed in the forward direction (Fig. 2a). The recoil to binary peak ratio decreases with increase in the projectile energy (Figs. 2a-2c), however the recoil peak still being larger than binary peak. The magnitude of binary and recoil peaks decrease and the peak positions also shifts towards higher ejected electron angles with increase in the momentum transfer however the magnitude decrement and shifting of position is more at the higher incident electron energies. The trends of TDCS for the inner shell ionization of beryllium atoms are significantly different from the outer shell ionization however similarity is observed with the trends of TDCS for He

atoms (Fig. 1d) due to ionization taking place from 1s orbital. The dominant recoil peaks for the ionization from 1s orbital may be attributed to the increased nucleus interaction. The binary and recoil peaks are observed in the nearly same direction of momentum transfer and its opposite in the standard DWBA results.

The TDCS results for the ionization of $Be^{2+}$(1s) are presented in Figure 3 and 4 at different sets of energies and momentum transfer conditions in the standard DWBA (red solid curves). The TDCS results for He atoms have also been calculated and compared for the similar kinematics, however polarization potential and PCI have been included in the standard DWBA for helium atoms in Figure 3 (black solid curves). The polarization potential and PCI have not been found significant for the ionization of $Be^{2+}$ target due to higher incident electron energy and very small dipole polarizability. The polarization potential and PCI have also not been significant for the ionization of He atoms at higher incident electron energies used in Figure 4 so standard DWBA results are plotted (black solid curves). The present DWBA results have been compared with the experimental data [40-41] obtained for the ionization of helium atoms for the similar kinematical conditions. Results of TDCS for $Be^{2+}$(1s) are presented at incident electron energy 231 eV in Figure 3. TDCSs have been calculated for two different sets of outgoing electrons energies ($E_1$=67 eV; $E_2$=10 eV and $E_1$=72 eV; $E_2$=5 eV) at scattering angels $15^0$ and $20^0$. The calculated TDCS for $Be^{2+}$(1s) have been compared with the experimental TDCS for He(1s) target [40] and TDCSs calculated for He atoms (incident electron energy 102 eV). The experimental data have been normalized independently to the TDCS results for He atoms (black solid curves) for the best visual fit. Two peak structure similar as He (1s) is observed in the trends of TDCS for $Be^{2+}$(1s) target. The calculated TDCSs for He atoms show reasonable agreement with the measurements with certain discrepancy in the recoil peak agreement, however nearly same recoil to binary peak ratio and nearly same binary peak positions are observed. Similarity in the trends of TDCS is observed for $Be^{2+}$ and He targets with the expected shift in the peak positions. The binary emission of electron becomes stronger as scattering angle is increased for the ionization of both the targets showing smaller recoil to binary peak ratio, however recoil emission remains dominant with slight decrease in the recoil to binary peak ratio for $Be^{2+}$(1s) target. The trends of TDCS clearly indicate the effect of nuclear charge for the ionization taking place from the targets of similar electronic configurations. The binary peaks in the experimental TDCS as well as the calculated TDCS for He (1s) is shifted away from the momentum transfer direction however the recoil peaks are obtained in the nearly same direction of opposite to the momentum transfer in the calculated TDCS. Both the binary and recoil peaks are shifted towards higher ejected electron angles in the calculated TDCS for $Be^{2+}$(1s) target.

TDCS calculated in the standard DWBA for $Be^{2+}$ are presented in Figure 4 for the ejected electron energies 37 eV, 74 eV and 205 eV at scattered electron energy 500 eV and scattering angle $-6^0$. The TDCSs for the He atoms have also been calculated in the standard DWBA and compared with the trends of calculated TDCS for $Be^{2+}$ and experimental TDCS for He [41]. The experimental data [41] have been normalized independently for the best visual fit in the binary peak region. The calculated TDCS for He atoms has good agreement with the

measurements [41]. The TDCS results for $Be^{2+}$ show similar trends as TDCS of He atoms with the binary peak for $Be^{2+}$ shifted towards lower ejected electron angles which agrees with the direction of momentum transfer. Higher recoil to binary peak ratio is observed in the TDCS structure of $Be^{2+}$ in comparison to the He case, however the binary peak is larger for both the targets as expected due to higher projectile energies. The trend of larger recoil peaks for $Be^{2+}$ target signifies the role of nuclear charge and it is observed more dominantly with recoil peak even larger than binary peak at relatively lower energies (Figure 3). The magnitudes of recoil peaks may not be directly compared for the $Be^{2+}$ and He due to different ratios of incident energy to ionization potential (IP).

It is interesting to observe the trends of TDCS for the ionization of $Be^{+}(2s)$ targets, which are very different from the ionization of $Be^{2+}(1s)$ (Figure 5). The electron impact TDCSs for $Be^{+}(2s)$ target have been compared with the experimental TDCS for Li(2s) atoms [42], present calculated TDCS for Li(2s) atoms, other available theoretical TDCSs for Li(2s) atoms [43, 44] and TDCS results for $Be^{+}(2s)$ [38]. The TDCSs for $Be^{+}(2s)$ and Li(2s) have been calculated in the DWBA formalism including polarization potential and PCI. We observe that apart from the recoil and binary peaks more structures are observed for both the $Be^{+}(2s)$ and Li(2s) targets which may be due to the radial node of 2s orbital wave function. The TDCS results are presented for the equal energy sharing $E_1 = E_2 = 47.3$ eV between two outgoing electrons in Figure 5a and unequal energy sharing in Figure 5b ($E_2 = 23.6$ eV). Present TDCS results calculated for Li(2s) atoms agree well with the measurements as well as with the other available theoretical results [43, 44]. Similarities in the trends of TDCS for $Be^{+}(2s)$ and Li(2s) targets are observed and the differences may be attributed to the different nuclear charges. The TDCS results for the $Be^{+}(2s)$ are presented at incident electron energy 72.0 eV in Figure 5c. The present TDCS results calculated using DWBA with polarization potential and PCI (red solid curve) and standard DWBA (dashed curve) are compared with the available theoretical TDCS [38] calculated in the Coulomb Born approximation (CBA) with effective charges and scaling laws. All the theoretical results show more than two peaks in the TDCS structure with dominant recoil and binary peaks of nearly same magnitude. Present DWBA results with polarization potential and PCI agree well with the theoretical results calculated earlier [38]. The deep minimum observed in the TDCS [38] around ejected electron angle $\theta_2 = 305^0$ is of further interest, a minimum in the TDCS structure is also observed in the present calculated results around similar angular position but not so deep. The trends of TDCS observed for Li(2s) and $Be^{+}(2s)$ targets may also have sensitive dependence on the projectile energy, which could be inferred from the TDCS trend obtained for Li(2s) atoms at relatively higher energy $E_0 = 958$ eV in earlier study [53].

The trends of TDCS have been compared for Be(2s), $Be^{+}(2s)$, $Be^{2+}(1s)$ and He(1s) targets for the similar kinematic conditions (Figure 6). The TDCS results for Be(2s), $Be^{+}(2s)$ and He(1s) have been calculated in DWBA approach with polarization potential and PCI, however the TDCS for $Be^{2+}(2s)$ has been calculated in standard DWBA. The trends of TDCS for $Be^{2+}(1s)$ target (black solid curve in Fig. 6a) is nearly similar as He(1s) target (red solid curve in Fig. 6a), which are

iso-electronic targets. However the recoil to binary peak ratio is larger for the $Be^{2+}$(1s) target due to higher nuclear charge. To test the effect of nuclear charge we have calculated TDCS for the $Be^{2+}$ target with the charge of He (red solid curve in Fig. 6b) and TDCS of He target with the charge of Be (black solid curve in Fig. 6b). A larger binary peak is observed for $Be^{2+}$ with reduced nuclear charge however a large recoil peak with even some splitting is observed for the He with higher nuclear charge. The effect of nuclear charge is also visible in the TDCS trends of $Be^{2+}$ target in Figure 3 and 4. Finally, the trends of TDCSs are compared for the ionization of $Be^{2+}$(1s) and Be(1s) in Figure 7 for equal energy sharing between the two outgoing electrons. TDCSs for both the targets have been calculated in standard DWBA since the polarization and PCI has not been found significant at the incident electron energy 200 eV and also due to very small dipole polarizability of $Be^{2+}$. Comparison of trends of TDCS for $Be^{2+}$(1s) and Be(1s) helps to understand the similarities / differences in the inner and outer shell ionization of targets having similar nuclear charge. Larger recoil peaks are observed for both the targets.

## IV Conclusions

The electron impact ionization cross sections are reported for the beryllium atoms and its charged states ($Be^{2+}$ and $Be^{+}$) for the coplanar emission of electrons. At the low incident electron energy apart from the binary and recoil peaks more peaks are observed in the TDCS for the ionization of beryllium atoms. The observed peaks shift towards higher ejected electron angles with increase in the momentum transfer. The polarization potential and PCI has been found significant at the lower energies and inclusion of these effects produce shift of the binary and recoil peaks from the direction of momentum transfer and its opposite. Strong recoil emission of electron is observed for the inner shell ionization of beryllium atoms at a very small ejected electron energy which is due to the interaction of nuclear charge. Rapid decrease of recoil as well as binary peak magnitude is observed with the increase of momentum transfer as incident electron energy increases for the ionization taking place from the 1s orbital of neutral beryllium. The trends of TDCS for the ionization of $Be^{2+}$(1s) have been compared with the experimental and calculated TDCS of He(1s) atoms in the intermediate to high incident electron energy ranges. Similarities in the trends of TDCS are observed for the ionization of $Be^{2+}$ with stronger recoil peaks due to the effect of nuclear charge. Both the binary and recoil peaks are shifted away from the direction of momentum transfer at the intermediate energy and the peaks are observed in the direction of momentum transfer at the higher energies which indicates the requirement of full form of exchange potential at low and intermediate energies, however the localized version may be sufficient at the higher incident electron energies. Nice agreement between the present calculated TDCS and earlier reported TDCS is obtained for the ionization of $Be^{+}$ targets, however deep minimum present in the TDCS of [38] requires further investigation. Similarities in the trends of TDCS for $Be^{+}$(2s) and Li(2s) are obtained, however the present calculated TDCS for Li atoms produced reasonable agreement with the available measurements and theoretical results. The calculated TDCS for neutral beryllium atoms has also been compared with the TDCS obtained for the ionization of its charged states in the same kinematic conditions. The trends of TDCS for the $Be^{2+}$(1s) match well with the trends of TDCS for the Be(1s) and He(1s), which is the orbital effect.

Present attempt helps to understand the collision dynamics of alkali earth metal beryllium and its charged states. The ionization taking place from the targets Be(2s), Be(1s), $Be^{+}$(2s) and $Be^{2+}$(2s) is investigated which have respectively 4, 3 and 2 electrons. Target polarization and PCI effects have been found significant for the Be(2s) and $Be^{+}$(2s) targets at lower projectile energies however these effects are not significant for the ionization of Be(1s) and $Be^{2+}$(2s) as projectile energies are higher (IPs 128.0 eV and 154.0 eV respectively) and value of dipole polarizability for $Be^{2+}$(2s) is very small. The Important information about the trends of TDCS have been obtained through the possible comparison between the trends of experimental TDCS for He and Li targets for the iso-electronic targets ($Be^{2+}$ and $Be^{+}$), and also the comparison of trends of the calculated TDCS. The similarities / differences are marked for the ionization of iso-electronic and iso-nuclear targets and the possible factors such as nature of wave function, nuclear charge, and shell dependence are analyzed. It is hoped that these calculations will stimulate more experimental and theoretical work for the differential cross sections of alkaline earth metal and its ions in continuation of the already existing excellent work for helium atoms.

## Acknowledgments

GP acknowledges JSPS Long Term Fellowship AY 2017 (L17538) provided by Japan Society for Promotion of Science. GP also acknowledges National Institute for Fusion Science (NIFS), Toki Japan for providing hospitality and Sir Padampat Singhania University (SPSU), Udaipur, India for providing sabbatical leave.

## References

[1] V. Vahedi and M. Surendra, Comput. Phys. Commun. 87, 179 (1995).
[2] ITER 2016 (http://iter.org/mach/blanket)
[3] G. Federici, Phys. Scr. T **124**, 1 (2006)
[4] R. Doerner, M.J. Baldwin, D. Buchenauer, G. De Temmerman, D. Nishijima, J. Nucl. Mater. **390**, 681 (2009)
[5] C. Bjorkas, K. Vortler, K. Nordlund, D. Nishijima, R. Doerner, New J. Phys. **11**, 123017 (2009)
[6] D. V. Fursa and I. Bray, J. Phys. B: At. Mol. Opt. Phys. 30, 5915 (1997).
[7] K. Bartschat, P. G. Burke and M. P. Scott, J. Phys. B: At. Mol. Opt. Phys. 30, 5915 (1997)
[8] C. P. Balance, D. C. Griffin, J. Colgan, S. D. Loch and M. Pindzola, Phys. Rev. A 68, 062705 (2003).
[9] J. Colgan, S. D. Loch, M. S. Pindzola, C. P. Balance and D. C. Griffin, Phys. Rev. A 68, 032712 (2003).
[10] W.C. Fon, K.A. Berrington, P.G. Burke, V.M. Burke, and A. Hibbert, J. Phys. B 25, 507 (1992).
[11] R.E.H. Clark and J. Abdallah, Phys. Scr., T T62, 7 (1996).
[12] K. Bartschat, P.G. Burke, and M.P. Scott, J. Phys. B 29, L769 (1996).
[13] D.V. Fursa and I. Bray, J. Phys. B 30, L273 (1997).
[14] O. Zatsarinny, K. Bartschart, D. V. Fursa and I. Bray, J. Phys. B: At. Mol. Opt. Phys. 49, 235701 (2016).

[15] H. P. Summers, M. von Hellerman, F. J. de Heer and R. Hoekstra, Nucl. Fusion (Supplement) 3, 7 (1992).
[16] J. Mitroy and D.W. Norcross, Phys. Rev. A 37, 3755 (1988).
[17] K.A. Berrington and R.E.H. Clark, Nucl. Fusion Suppl. 3, 87 (1992).
[18] K. Bartschat and I. Bray, J. Phys. B 30, L109 (1997).
[19] A.K Pradhan, D.W. Norcross, and D.G. Hummer, Phys. Rev. A 23, 619 (1981).
[20] N.R. Badnell, J. Phys. B 28, 955 (1985).
[21] C.P. Ballance, N.R. Badnell, and E.S. Smyth, J. Phys. B 36, 3707 (2003).
[22] J.C. Chang, H. L. Sun, W.Y. Cheng and K.-N. Huang, Phys. Rev. A 69, 052713 (2004).
[23] W.M. Huo, Phys. Rev. A 64, 042719 (2001).
[24] M.Alfaz Uddin, A.K.F. Haque, M.S. Mahbub, K.R. Karim, A.K. Basak, B.C. Saha, Int. J. of Mass Spect. 244, 76 (2005).
[25] M.A. Uddin, A.K.F. Haque, A.K. Basak, B.C. Saha, Phys. Rev. A 70, 032706 (2004).
[26] T. Maihom, I. Sukuba, R. Janev, K. Becker, T. Mark, A. Kaiser, J. Limtrakul, J. Urban, P. Mach, and M. Probst, Eur. Phys. J. D 67, 2 (2013).
[27] P.O. Taylor, R.A. Phaneuf, and G.H. Dunn, Phys. Rev. A 22, 435 (1980).
[28] R. Wehlitz and S. B. Whitfield, J. Phys. B:At. Mol. Opt. Phys. 34, L719 (2001).
[29] A. J. Murray, Phys. Rev. A **72** 062711 (2005).
[30] Hitawala U, Purohit G and Sud K K 2008 J. Phys. B **41**, 035205.
[31] P. Bolognesi, H. Bohachov, V. Borovik, S. Veronesi, R. Flammini, E. Fainelli, A. Borovik, J. Martinez, Colm T. Whelan and H. R. J. Walters, J. Phys. B: At. Mol. Opt. Phys. 41, 015201 (2008).
[32] Y. Khajuria and P. C. Deshmukh, Phys. Rev. A **78** 024702 (2008).
[33] R. K. Chauhan, M. K. Srivastava and R. Srivastava, Phys. Rev. A **71** 032708 (2005).
[34] G. Purohit, V. Patidar and K. K. Sud, Phys. Scr. **80** (2009) 065301.
[35] J. Colgan and M. S. Pindzola, Phys. Rev. A 65, 022709 (2002).
[36] F. L. Yip, F. Martin, C. W. McCurdy and T. N. Rescigno, Phys. Rev. A 84, 053417 (2011).
[37] A. K. Kazansky and V. N. Ostrovsky, J. Phys. B: At. Mol. Opt. Phys. 30, L835 (1997).
[38] L. U. Ancarani and P-A Hervieux, J. Phys. B: At. Mol. Opt. Phys. 36, 4447 (2003).
[39] M Becher and B Joulakian, J. Phys. B: At. Mol. Opt. Phys. 42, 065206 (2009).
[40] M. Durr, C. Dimopoulou, A. Dorn, B. Najjari, I. Bray, D. V. Fursa, Z. Chen, D. H. Madison, K. Bartschat and J. Ullrich, J. Phys. B: At. Mol. Opt. Phys. 39, 4097 (2006).
[41] E. M. Staicu Casagrande, A. Naja, F. Mezdari, A. Lahmam-Bennani, P. Bolognesi, B. Joulakian, O. Chuluunbaatar, O. Al-Hagan, D. H. Madison, D. V. Fursa and I. Bray, J. Phys. B: At. Mol. Opt. Phys. 41, 025204 (2008).
[42] L. Frost, P. Freienstein, S. Hesse, W. Blask, G. Baum and W. Raith, 3rd European Conference on (e, 2e) collisions and related problems, invited papers and progress reports, ed. G. Stefani (CNR-IMAI, Rome, 1990) p. 295.
[43] R. Biswas and C. Sinha, Phys. Lett. A 206, 225 (1995).
[44] H. Hafid and B. Joulakian, Z. Phys. D 31, 49 (1994).
[45] E. Clementi and C. Roetti, At. Data Nucl. Data Tab. 14, 177 (1974).
[46] J. B. Furness and I. E. McCarthy, J. Phys. B 6, 2280 (1973).
[47] M. E. Riley and D. G. Truhlar, J. Chem. Phys. 63, 2182 (1975).
[48] I. E. McCarthy, Aust. J. Phys. 48 1 (1995).
[49] N. T. Padial and D. W. Norcross, Phys. Rev. A 29, 1742 (1984).

[50] J. P. Perdew and A. Zunger, Phy. Rev. B 23, 5048 (1981).
[51] S. J. Ward and J. H. Macek, *Phys. Rev. A*49, 1049 (1994).
[52] D. H. Madison and O. Al-Hagan, J. At. Mol. Opt. Phys. 2010, 367180 (2010).
[53] F. Elboudali and B. Joulakian, J. Phys. B: At. Mol. Opt. Phys. 34, 4877 (2001).

**Figure Captions**

Figure 1: TDCS plotted as a function of ejected electron angle for the ionization of Be(2s) at incident electron energy 31.0 eV and ejected electron energy 2.0 eV at different scattering angles (a) $2^0$ (b) $5^0$ and (c) $10^0$ (d) TDCS for He atoms at scattering angle $2^0$; Solid curve: DWBA results with polarization potential and PCI; dashed curve: DWBA results.

Figure 2: TDCS plotted as a function of ejected electron angle for the ionization of Be(1s) for ejected electron energy 2.0 eV at different scattering angles $2^0$ (solid line), $5^0$ (dashed line) and $10^0$ (dotted line) (a) $E_0$ = 200 eV (b) $E_0$ = 500 eV and (c) $E_0$ = 1000 eV

Figure 3: TDCS plotted as a function of ejected electron angle at incident electron energy 231 eV for different scattering angles shown in figure frames (a -b) $E_1$=67 eV; $E_2$=10 eV and (c-d) $E_1$=72 eV; $E_2$=5 eV. Red solid curve: DWBA results for $Be^{2+}$(1s); black solid curve: DWBA results with polarization potential and PCI for He(1s) and solid circles: experimental TDCS for He(1s) [40]. The experimental data have been normalized to the black solid curves independently for best visual fit.

Figure 4: TDCS plotted as a function of ejected electron angle at scattered electron energy 500 eV and scattering angle $-6^0$ (a) ejected electron energy 37 eV (b) ejected electron energy 74 eV and (c) ejected electron energy 205 eV. Red solid curve: DWBA results for $Be^{2+}$(1s); black solid curve: DWBA results with polarization potential and PCI for He(1s) and solid circles: experimental TDCS for He(1s) [41]. The experimental data have been normalized to the black solid curves independently for best visual fit.

Figure 5: TDCS plotted as a function of ejected electron angle at scattering angle $45^0$ (a) $E_1 = E_2$ = 47.3 eV (b) Incident electron energy 100 eV and ejected electron energy 23.6 eV; red solid curve: DWBA results with polarization potential and PCI for $Be^+$(2s); black solid curve: DWBA results with polarization potential and PCI for Li(2s); dashed curve: TDCS results for Li(2s) [43]; dotted curve: TDCS results for Li(2s) [44] and solid circles: experimental TDCS for Li(2s) [42]. (c) TDCS plotted as a function of ejected electron angle for $Be^+$(1s) at incident electron energy 72.0 eV, ejected electron energy 5.0 eV and scattering angle $1^0$; red solid curve: DWBA results with

polarization potential and PCI; dashed curve: DWBA results and black solid curve: TDCS results of [38].

Figure 6: (a) TDCS plotted as a function of ejected electron angle at incident electron energy 22.6 above IP. Dashed curve: DWBA results with polarization potential and PCI for Be(2s); Dotted curve: DWBA results with polarization potential and PCI multiplied by 8.3 for $Be^{+}$(2s); Solid black curve: DWBA results multiplied by 1255 for $Be^{2+}$(1s) and Solid red curve: DWBA results with polarization potential and PCI multiplied by 7.0 for He(1s). (b) TDCS plotted as a function of ejected electron angle at $E_1$=67 eV; $E_2$=10 eV and scattering angle $15^0$; Red solid curve: DWBA results for $Be^{2+}$(1s) with the nuclear charge of He; black solid curve: DWBA results for He(1s) with the nuclear charge of $Be^{2+}$(1s).

Figure 7: TDCS plotted as a function of ejected electron angle at $E_1 = E_2 = 51.0$ eV, $\theta_1 = 2^0$ Dashed curve: DWBA results for Be(1s) and Solid curve: DWBA results for $Be^{2+}$(1s).

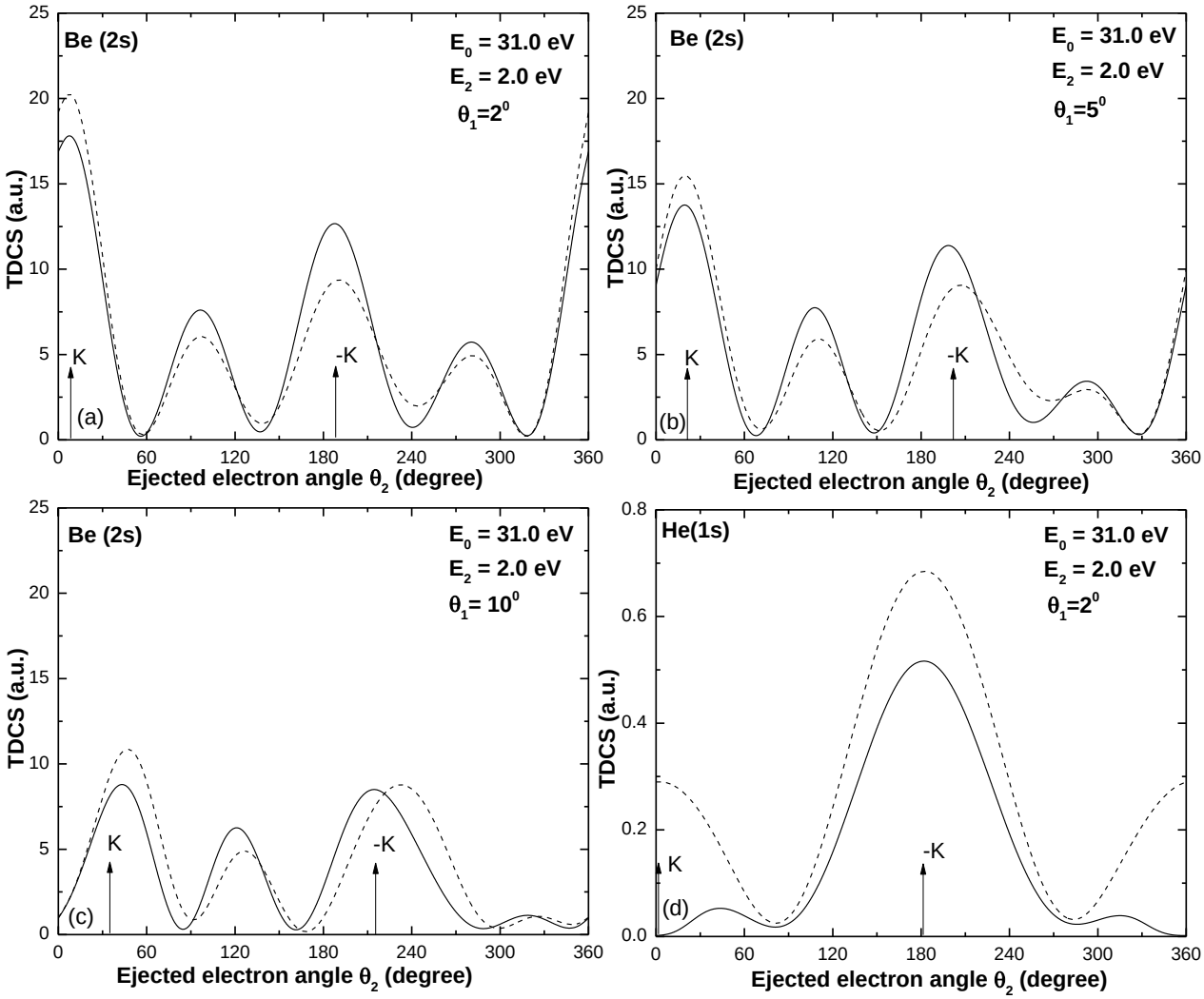
Be (2s)
E0 = 31.0 eV
E2 = 2.0 eV
θ1=2^0
TDCS (a.u.)
K
-K
(a)
Ejected electron angle θ2 (degree)
Be (2s)
E0 = 31.0 eV
E2 = 2.0 eV
θ1=5^0
TDCS (a.u.)
K
-K
(b)
Ejected electron angle θ2 (degree)
Be (2s)
E0 = 31.0 eV
E2 = 2.0 eV
θ1= 10^0
TDCS (a.u.)
K
-K
(c)
Ejected electron angle θ2 (degree)
He(1s)
E0 = 31.0 eV
E2 = 2.0 eV
θ1=2^0
TDCS (a.u.)
K
-K
(d)
Ejected electron angle θ2 (degree)

**Figure 1**

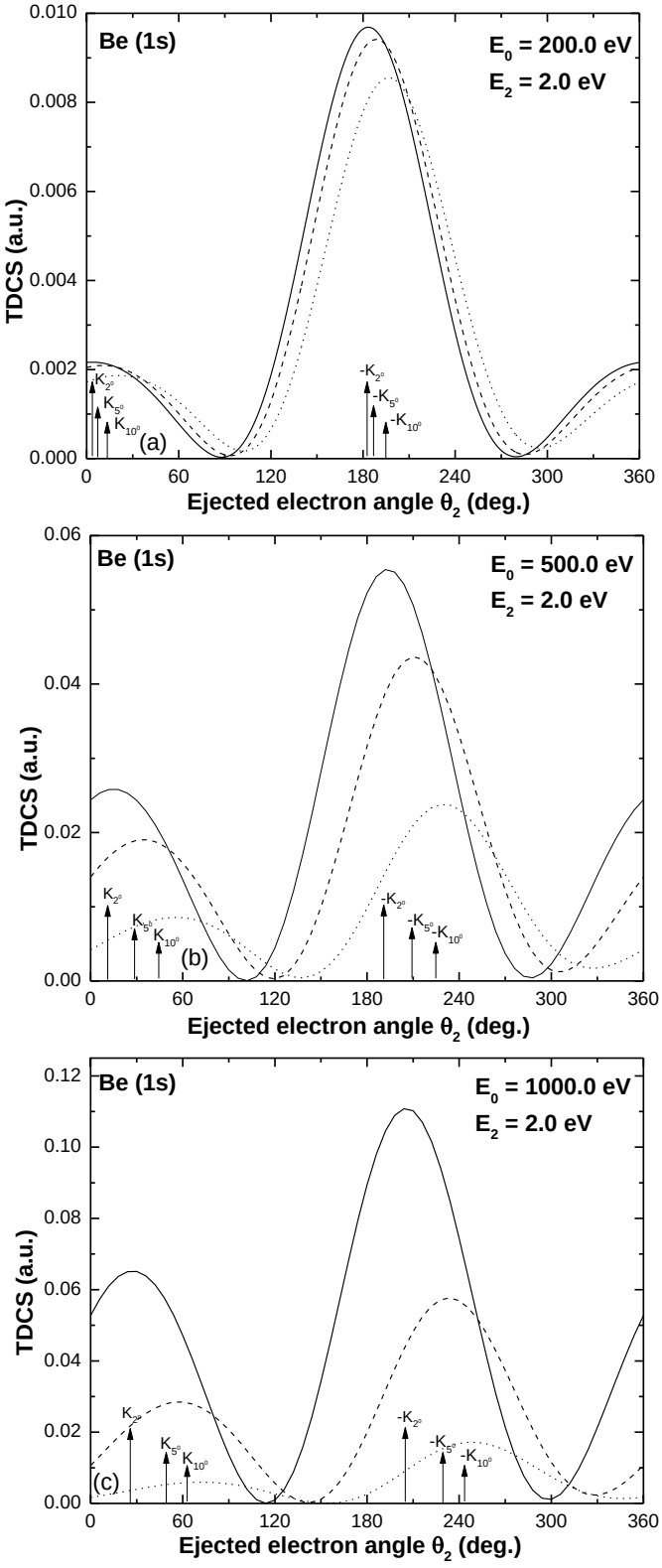
Be (1s)
E0 = 200.0 eV
E2 = 2.0 eV
TDCS (a.u.)
Ejected electron angle θ2 (deg.)
(a)
Be (1s)
E0 = 500.0 eV
E2 = 2.0 eV
TDCS (a.u.)
Ejected electron angle θ2 (deg.)
(b)
Be (1s)
E0 = 1000.0 eV
E2 = 2.0 eV
TDCS (a.u.)
Ejected electron angle θ2 (deg.)
(c)

**Figure 2**

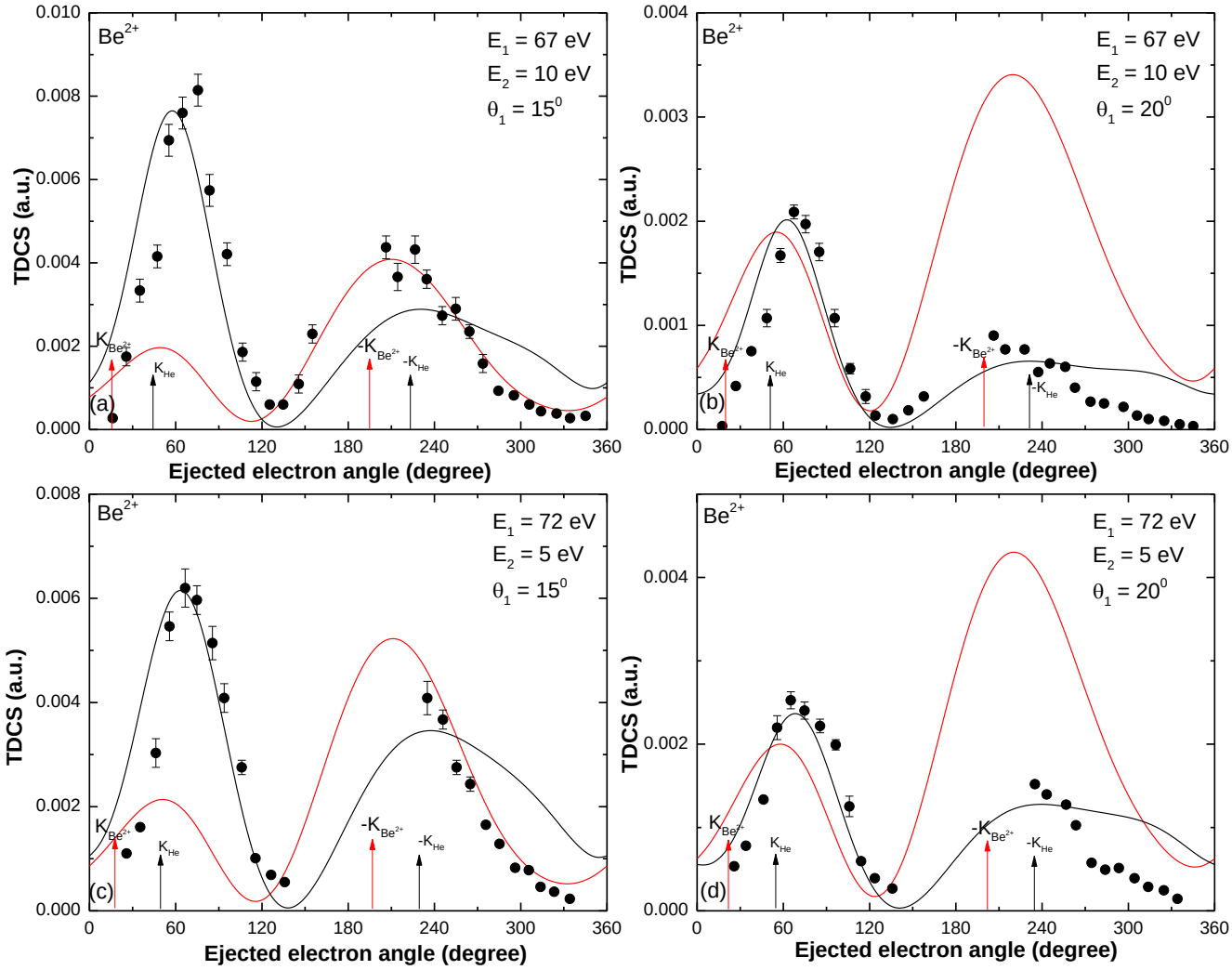
Be2+
E1 = 67 eV
E2 = 10 eV
θ1 = 150
(a)
Be2+
E1 = 67 eV
E2 = 10 eV
θ1 = 200
(b)
Be2+
E1 = 72 eV
E2 = 5 eV
θ1 = 150
(c)
Be2+
E1 = 72 eV
E2 = 5 eV
θ1 = 200
(d)
TDCS (a.u.)
Ejected electron angle (degree)
KBe2+
KHe
-KBe2+
-KHe

**Figure 3**

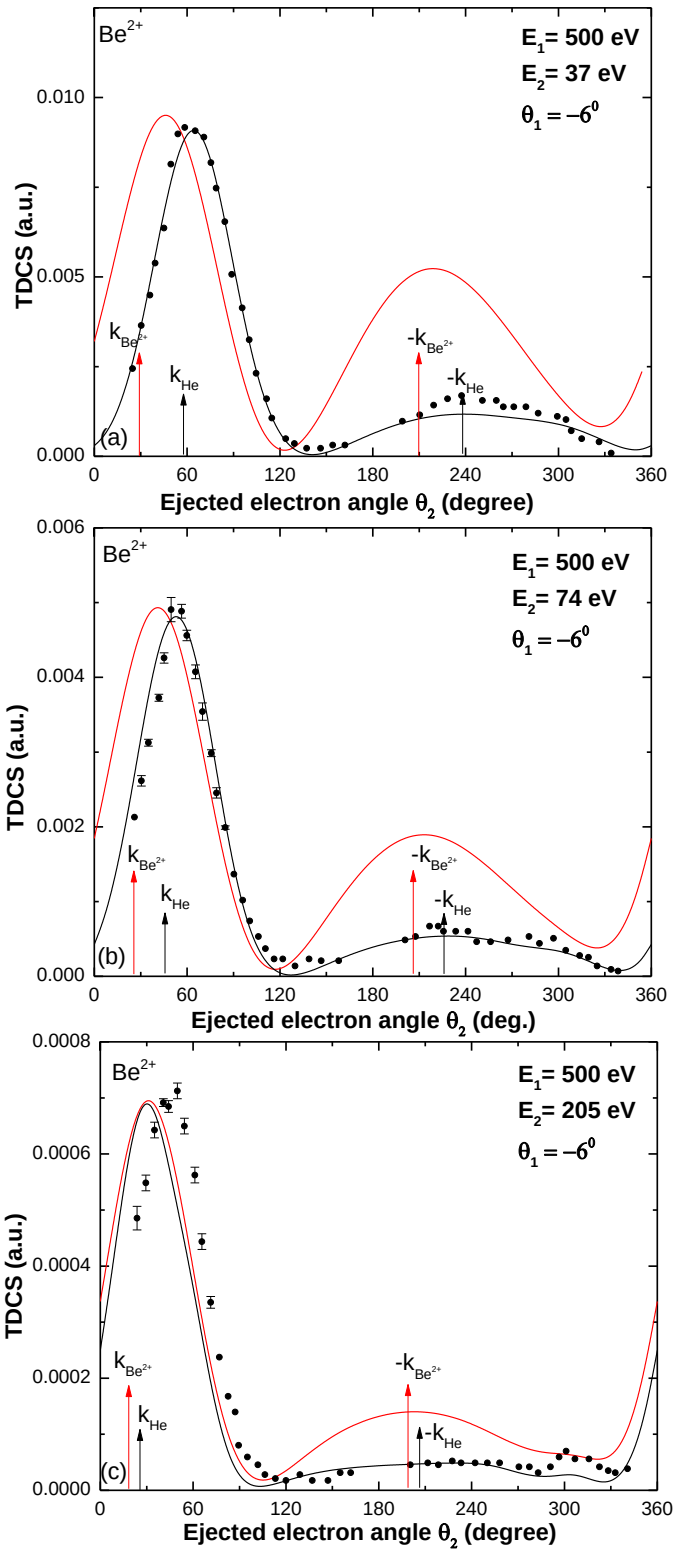
Be2+
E1= 500 eV
E2= 37 eV
θ1 = –6⁰
TDCS (a.u.)
0.010
0.005
0.000
kBe2+
kHe
-kBe2+
-kHe
(a)
0
60
120
180
240
300
360
Ejected electron angle θ2 (degree)
Be2+
E1= 500 eV
E2= 74 eV
θ1 = –6⁰
TDCS (a.u.)
0.006
0.004
0.002
0.000
kBe2+
kHe
-kBe2+
-kHe
(b)
Ejected electron angle θ2 (deg.)
Be2+
E1= 500 eV
E2= 205 eV
θ1 = –6⁰
TDCS (a.u.)
0.0008
0.0006
0.0004
0.0002
0.0000
kBe2+
kHe
-kBe2+
-kHe
(c)
Ejected electron angle θ2 (degree)

**Figure 4**

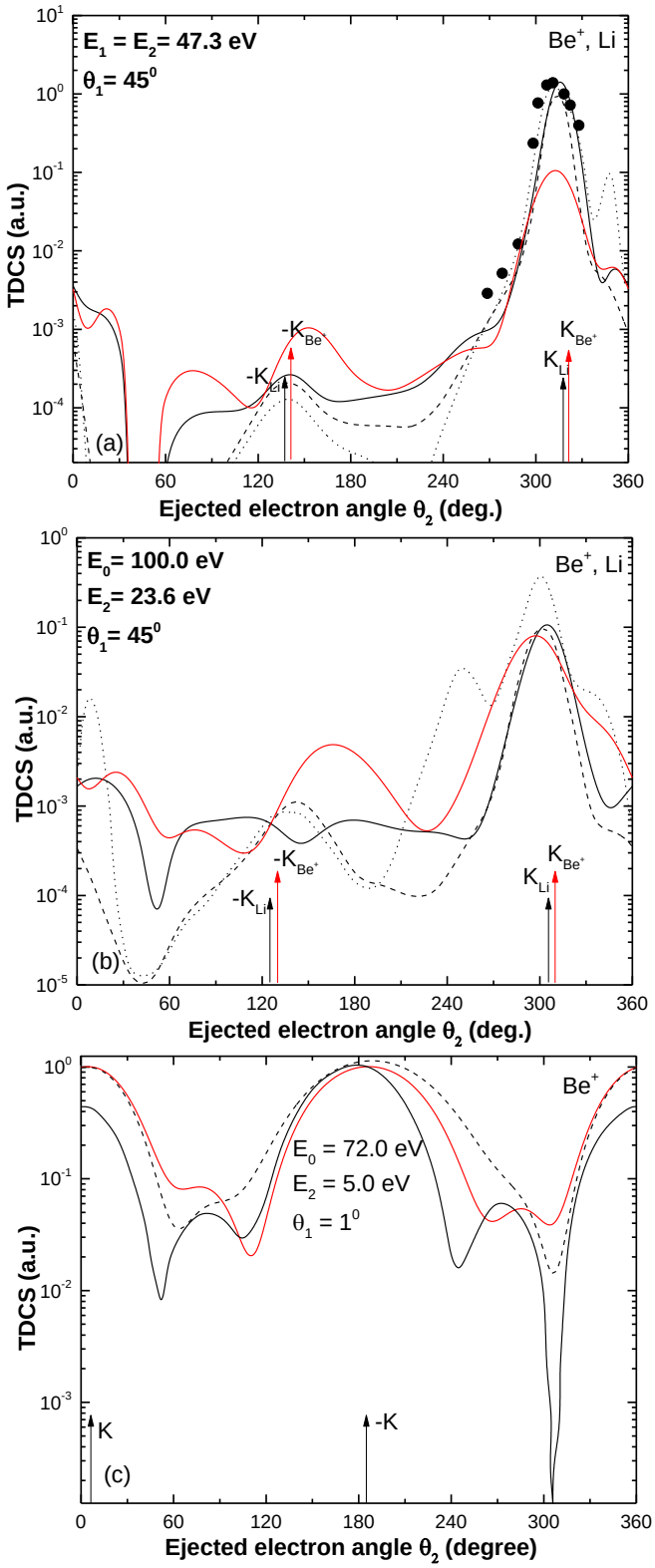
E1 = E2= 47.3 eV
θ1= 45⁰
Be+, Li
TDCS (a.u.)
-KBe+
-KLi
KBe+
KLi
(a)
Ejected electron angle θ2 (deg.)
E0= 100.0 eV
E2= 23.6 eV
θ1= 45⁰
Be+, Li
TDCS (a.u.)
-KBe+
-KLi
KBe+
KLi
(b)
Ejected electron angle θ2 (deg.)
Be+
E0 = 72.0 eV
E2 = 5.0 eV
θ1 = 1⁰
TDCS (a.u.)
K
-K
(c)
Ejected electron angle θ2 (degree)

**Figure 5**

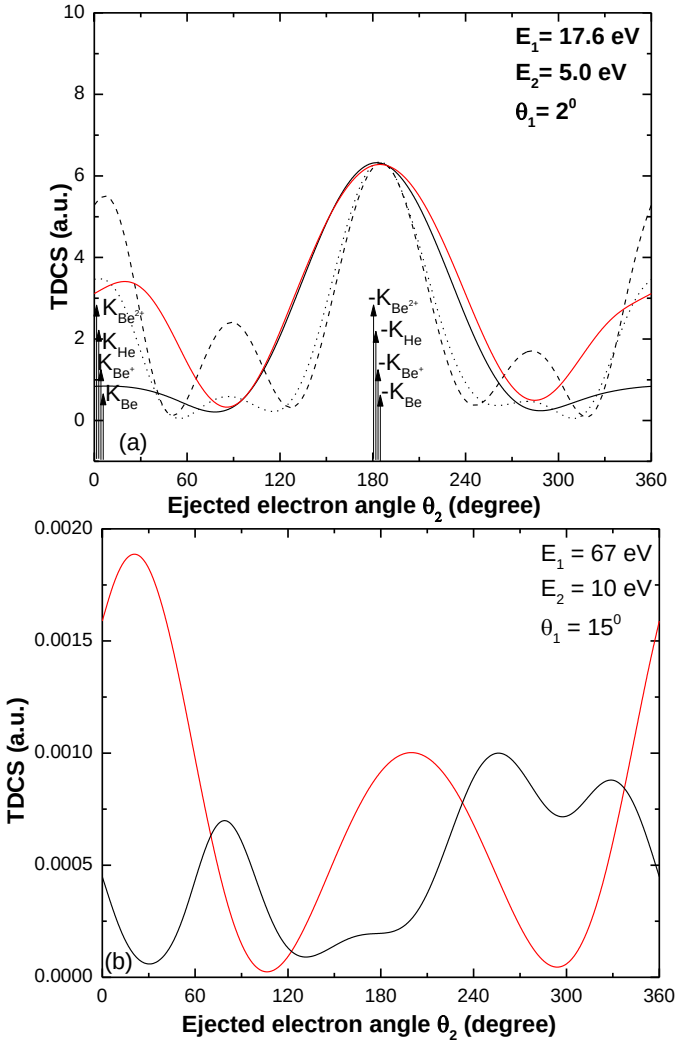
E1= 17.6 eV
E2= 5.0 eV
θ1= 2^0
TDCS (a.u.)
Ejected electron angle θ2 (degree)
(a)
E1 = 67 eV
E2 = 10 eV
θ1 = 15^0
TDCS (a.u.)
Ejected electron angle θ2 (degree)
(b)

**Figure 6**

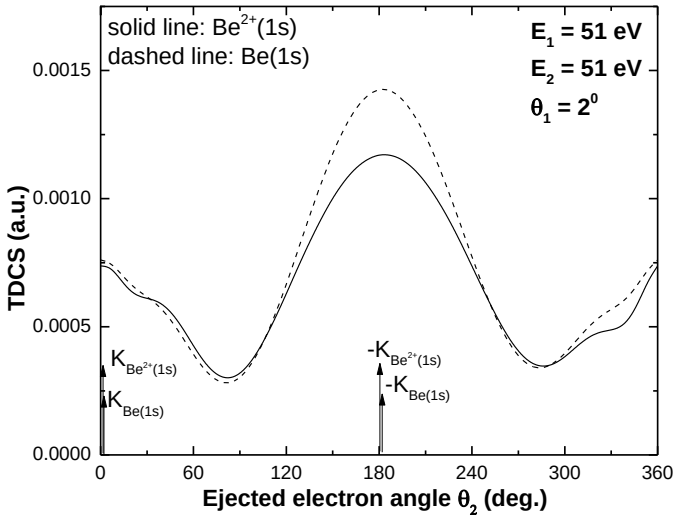
solid line: Be2+(1s)
dashed line: Be(1s)
E1 = 51 eV
E2 = 51 eV
θ1 = 20
TDCS (a.u.)
0.0015
0.0010
0.0005
0.0000
0
60
120
180
240
300
360
Ejected electron angle θ2 (deg.)
KBe2+(1s)
KBe(1s)
-KBe2+(1s)
-KBe(1s)

**Figure 7**